Water Research 190 (2021) 116676

Contents lists available at ScienceDirect

Water Research

journal homepage: www.elsevier.com/locate/watres

Enhanced arsenic removal from water by mass re-equilibrium: kinetics and performance evaluation in a binary-adsorbent system

Zhengyang Wang[a,b], Peng Liao[c], Xiaoqing He[d,e], Peng Wan[f], Bin Hua[g], Baolin Deng[a,*]

[a] Department of Civil and Environmental Engineering, University of Missouri, Columbia, Missouri 65211, USA
[b] Department of Environmental Sciences, The Connecticut Agricultural Experiment Station, New Haven, Connecticut 06504, USA
[c] State Key Laboratory of Environmental Geochemistry, Institute of Geochemistry, Chinese Academy of Sciences, Guiyang, 550081, P. R. China
[d] Electron Microscopy Core Facility, University of Missouri, Columbia, Missouri 65211, USA
[e] Department of Mechanical and Aerospace Engineering, University of Missouri, Columbia, Missouri 65211, USA
[f] Department of Chemical Engineering, University of Missouri, Columbia, Missouri 65211, USA
[g] Department of Agriculture and Environmental Science, Lincoln University, Jefferson City, Missouri 65102, USA

ARTICLE INFO

Article history:
Received 17 August 2020
Revised 9 November 2020
Accepted 24 November 2020
Available online 24 November 2020

Keywords:
Arsenic Removal
Adsorption Kinetics
Mass Transfer
Mass Re-equilibrium
Process Configuration

ABSTRACT

Because arsenic (As) is highly toxic and carcinogenic, its efficient removal from drinking water is essential. Considering some adsorption media may adsorb As fast but are too expensive to be applied in a household, while others could be abundantly available at low cost but with slow uptake kinetics, we explored a novel mass re-equilibrium (MRE) process between two media with different adsorption characteristics to enhance the overall As removal. We employed an adsorbent with fast adsorption kinetics to grab As from water, and then allow it to transfer to a second adsorbent with large capacity for As retention. In the system containing two adsorbents separated by a dialysis membrane, the results showed that As associated with a fast-adsorbing iron-based ordered mesoporous carbon could diffuse to a slow-adsorbing but high-capacity iron-based activated carbon. Column tests were further conducted, showing that the mixed medium, composed of the two adsorbents, could be used to adsorb As at a very short empty bed contact time ($\leq$ 1 min) and the removal was improved by the MRE that potentially redistributed solid-phase As during pump-off periods. This study points to a new direction that by the MRE process, novel binary-adsorbent approaches may be developed for contaminant removal, if suitable media and process configuration could be identified.

1. Introduction

Since the severe arsenic (As) contamination in Bangladesh was uncovered more than two decades ago (SenGupta et al., 2017), tremendous efforts have been devoted to mitigating this problem in the world (Cui et al., 2013; Möller et al., 2009; Neumann et al., 2013; Peter et al., 2017; Xie et al., 2017). The As challenge, however, still exists in many developing (Cui et al., 2013; Schaefer et al., 2016) and developed (McGrory et al., 2017; Middleton et al., 2016; Yan and Flanagan, 2017) countries. Adsorption is one of the most effective approaches for As removal due to its operational simplicity and small footprint. The removal of As by various media has been extensively studied, including iron (Fe)-impregnated carbons (Wang et al., 2019b). As adsorption is a ligand exchange process with complexes formed on the surface with reactive Fe moieties (Fendorf et al., 1997; Sherman and Randall, 2003). A simulation demonstrated that such a reaction proceeds with three energetically-favorable steps that progress from physical adsorption, to monodentate complexation, and finally to bidentate complexation (Farrell and Chaudhary, 2013). Facing the long-existing As problem, revisiting treatment processes with adsorption is a must.

Decentralized water treatment systems, such as point-of-use (POU) units, have been widely used to produce safe drinking water (Pérez-Vidal et al., 2016; Peter et al., 2017; Sankar et al., 2013). In POU systems, the required hydraulic contact time is, e.g., 32 seconds in one study (Möller et al., 2009), an order of magnitude shorter than the necessary contact time of conventional adsorption towers in community water treatment plants (Chen et al., 2007; Tresintsi et al., 2013). Though adsorbents with rapid As adsorption kinetics have been developed, including Fe-impregnated ordered mesoporous carbon (Wang et al., 2019b), nanoscale Fe/mesoporous carbon composite (Baikousi et al., 2015), hybrid microspheres (Moraga et al., 2019), metal-organic frameworks (Wang et al., 2019a), and nanomaterials (Mertens et al., 2016; Yang et al., 2010; Zhao et al., 2016), the cost of these

* Corresponding author.
E-mail address: dengb@missouri.edu (B. Deng).

https://doi.org/10.1016/j.watres.2020.116676
0043-1354/

adsorbents is prohibitively high and very few of them can reach the market. On the other hand, many other low-cost adsorbents have been examined, such as modified geomedia (Ray et al., 2019), tailored biochars (Bakshi et al., 2018; Hu et al., 2015), and Fe-impregnated granular activated carbon (Kalaruban et al., 2019). However, because of the slow uptake rates, their application in POU systems is rather limited. The focus of this study is therefore to explore if we could integrate these two types of adsorbents with an innovative process configuration for the enhanced As removal.

This exploration was partially inspired by the work from Morel and Hering (Morel and Hering, 1993) who established a pseudo-equilibrium model describing a competitive relationship between two ligands with a metal ion. The pseudo-equilibrium could be reached quickly with the ligand possessing a rapid complexation kinetics, but the system eventually proceeded to a true equilibrium with the one that had a slower kinetics but a higher affinity, by replacing the initially-complexed ligand (see details in section 3.3). By analogy, we hypothesized that it was possible to use two media, one with fast adsorption kinetics but low affinity, and the other slow kinetics but high affinity, to remove a contaminant more efficiently. The re-equilibrium would involve in the contaminant transfer from the fast-adsorbing medium to the one with a slower adsorption kinetics.

Specifically for arsenate (As(V)) adsorption, the concept of this mass re-equilibrium (MRE) can be illustrated by the following two reactions:

$$\equiv M'As \rightleftarrows \equiv M' + As \quad (1)$$

$$\equiv M'' + As \rightleftarrows \equiv M''As \quad (2)$$

where As(V) in pseudo-equilibrium with the faster adsorption surface ($\equiv M'$) could be transferred to the slower but stronger adsorbing surface ($\equiv M''$). The use of the mixed medium may therefore result in an overall fast kinetics, high capacity, and affordable application cost. This MRE concept is analogous to the information storage system in a computer where a cache buffer is used to quickly store and transfer information, while a disk platter to store copious quantities of data (Fig. 1).

The goal of this study was to test our hypothesis that the MRE process between two adsorbents could be used for the enhanced As(V) removal. Specific objectives were to: 1) investigate As(V) adsorption kinetics and capacities on various Fe-based carbons to select suitable media for the MRE process evaluation; 2) monitor As(V) transport between different media in a batch-scale reactor (refer to Fig. 1); 3) understand the MRE process using batch experimental data and solid sample characterizations; and 4) evaluate the feasibility of engineering MRE process in well-packed column experiments.

2. Experimental

2.1. Chemicals

Sodium arsenate ($Na_2HAsO_4 \bullet 7H_2O$), sodium nitrate ($NaNO_3$), sodium hydroxide (NaOH), ferric nitrate ($Fe(NO_3)_3 \bullet 9H_2O$), Pluronic® F-127 (MW = 12600, EO_{106}-PO_{70}-EO_{106}), phenol, formalin (37 wt. % formaldehyde), 3-(N-morpholino)propanesulfonic acid (MOPS), ammonium persulfate, 1, 10-phenanthroline, and hydroxylamine hydrochloride were purchased from Sigma-Aldrich. Concentrated HNO_3, HCl, and H_2SO_4 were procured from Fisher. All chemicals were of reagent grade. Arsenic stock solution (500 mg As/L) was prepared from $Na_2HAsO_4 \bullet 7H_2O$, and then filtered through 0.45 μm cellulose membrane. Milli-Q water (18.2 MΩ•cm) was used to prepare solutions.

2.2. Preparation of Fe-based carbonaceous adsorbents

Three types of carbons were selected for the study, based on their differences in particle size and porous structure (Table S1

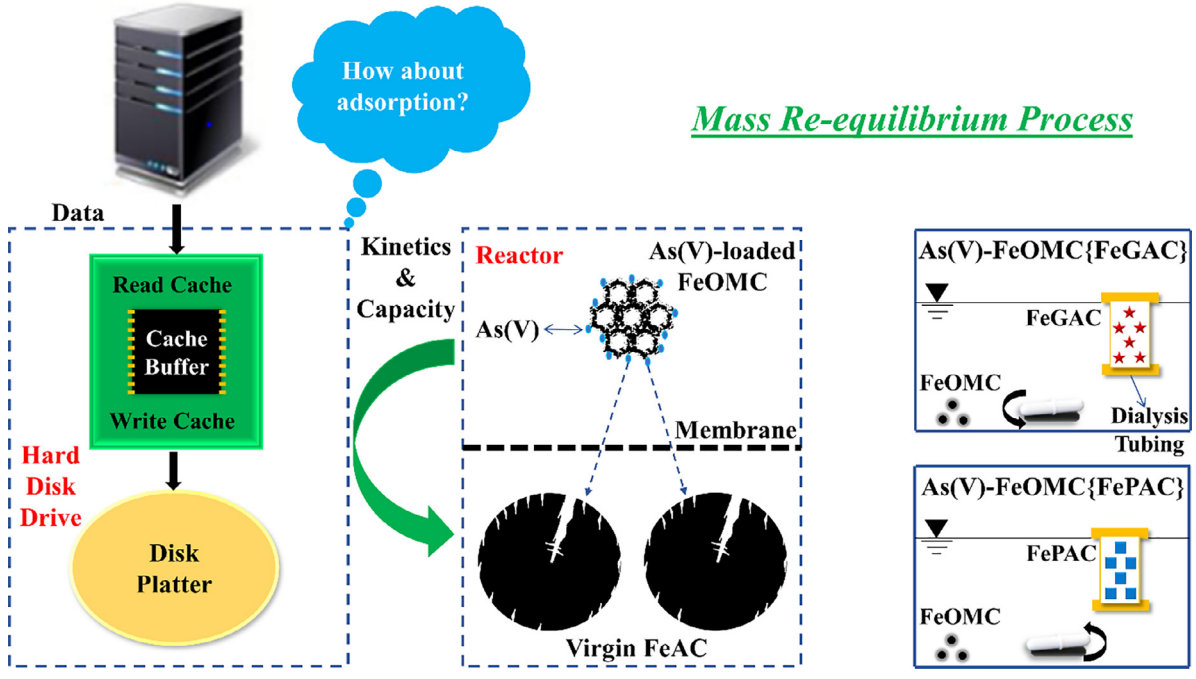

Fig. 1. A schematic illustrating the dual media system for As(V) adsorption. Adsorption kinetics and capacity are compared to the information storage in computer cache and disk platter. In a hard disk drive, data are transferred from fast-reading cache to large-storage disk platter. Similarly, during the MRE process, As(V) loaded on fast-adsorbing FeOMC is transferred to virgin FeACs with larger compacities. Media are separated by a dialysis tubing in a glass dish. In the experiments of As(V)-FeOMC{FeGAC} and As(V)-FeOMC{FePAC}, the small black dots denote the As(V)-loaded FeOMC in the bulk solution and "{}" represents the dialysis tubing where granular FeAC (FeGAC) or powdered FeAC (FePAC) is confined.

of Supplementary Materials): ordered mesoporous carbon (OMC), granular activated carbon (GAC), and powdered activated carbon (PAC). By oxidizing all carbons for both 12 h and 24 h respectively, six carbon samples were acquired (see Text S1 and Figs. S1-S2 for details). The oxidation was to aid Fe impregnation that followed a reported protocol (Chen et al., 2007). Briefly, 2.0 g of oxidized carbons were mixed with 200 mL of 0.10 M $Fe(NO_3)_3$ solution at pH 2.0 for 1.5 h. Suspensions were heated at 96 ± 1°C until dry, and then the dry solids were washed thoroughly. The prepared adsorbents were named with subscripts indicating the average Fe contents, i.e., Fe_3OMC, Fe_6GAC, and Fe_{23}PAC denoted the contents of 3.05%, 6.51%, and 23.2%, respectively.

2.3. Batch experiments: As(V) adsorption

The prepared adsorbents were firstly assessed in batch tests for their As(V) adsorption characteristics. Batch tests were conducted with 20-mL capped glass vials at room temperature (22 ± 1°C), and all working solutions contained 50.0 mM $NaNO_3$ as background electrolyte. Final pH was controlled at 6.6 ± 0.1 by 2.0 mM MOPS buffer, which did not interfere with As(V) adsorption on Fe minerals (Couture et al., 2013; Wolthers et al., 2005).

Preliminary tests were carried out to identify adsorbents with different adsorption kinetics. The empirical pseudo-first-order rate constants were firstly compared between two candidates from the same parent carbon, and the faster one was selected for all remaining experiments (Table S2).

Kinetic experiments were performed by adding 10.0 mg adsorbent into 10.0 mL of 49.9-51.0 μg As/L solutions. The suspensions were stirred at 500 rpm on a magnetic stirrer and the supernatants were sampled to monitor the change of As concentration as a function of time. For FeOMCs and FePACs, the adsorption equilibrium was reached in 20 and 30 min, respectively, while for FeGACs, it took 12 h (data not shown). Additional kinetic tests lasting for 24-hour were conducted for Fe_3OMC and Fe_6GAC, in which 5.0 mg of each medium was dosed to 10.0 mL of 2.17 mg As/L solutions in separate 20-mL glass vials and then were mixed on an end-over-end shaker (Glas-Col, Terre Haute) at 50 rpm. Samples were taken at 0.1, 0.3, 0.7, 1, 3, 6, 9, 12, 15, 18, and 24 h for As analysis following filtration by 0.22 μm polyethersulfone (PES) membranes.

Adsorption isotherms were measured with the bottle-point method (Schideman et al., 2006). All suspensions with predetermined As to solid ratios were mixed on the shaker at 50 rpm for 24 h prior to As analysis. Controlled experiments with virgin carbons were also conducted in duplicate.

2.4. Dialysis experiments: MRE assessment

Experimental set-up to evaluate MRE is shown in Fig. 1. Duplicate experiments were carried out at room temperature with the same pH and background electrolyte as the batch tests. Data were reported as means unless otherwise specified. The first step was to couple As-loaded adsorbent with virgin ones. Explicitly, 30.0 mg of Fe_3OMC was mixed with 30.0 mL of 48.5-50.6 mg As/L working solutions in centrifuge tubes at 50 rpm on the shaker for 24 h, and then were centrifuged at 10,000 rcf at 22°C for 20 min. Afterwards, 29.5 mL of supernatants were drawn with pipette, leaving 0.5 mL in the centrifuge tubes. A sample, named as Solution I, was taken by filtering the supernatant through a 0.22 μm PES membrane. The amount of As(V) loaded to Fe_3OMC, reported as the amount at day 0, was calculated by the As concentration difference between the initial working solution and Solution I. Another replicate was sacrificed to obtain a freeze-dried solid sample for characterizations.

A glass dish (Fig. S3) was filled with 50.0 mL solution with 50.0 mM $NaNO_3$ and 2.0 mM MOPS (named as Solution II). 60.0 mg of virgin adsorbent (Fe_6GAC or Fe_{23}PAC) was placed into a cellulose dialysis tube (7-8 cm length and 3.4 cm flat width) with a molecular weight cut-off of 50 kDa (Spectra/Por® 6, Spectrum). After the tubing with the virgin adsorbent was moved into the dish, the As-loaded Fe_3OMC was transferred to the reactor along with 0.5 mL supernatant. Solution II was again used to transfer the trace amount of leftover in the centrifuge tube. Only an extra 8.0 mL of Solution II was allowed, indicating the total volume of 58.5 mL at the beginning.

The reactor was covered by a parafilm and then a foil, magnetically stirred at 600 rpm for 1, 3, and 5 day. Control experiments, Fe_3OMC{Solution II} ("{}" = dialysis tubing), were performed for 1 and 5 day to account for desorption of As(V) from Fe_3OMC without the other adsorbent in the reactor. When the reaction was completed, supernatant was carefully withdrawn and filtered through a 0.22 μm PES membrane to collect Solution III. Total As of Solution III was analyzed for the liquid-phase As amount after MRE reaction, with all analytical details for Solutions I, II, and III described in Table 1.

After taking the dialysis tubing out of the reactor, particles were transferred, with the supernatant if needed, and vacuum filtered through a 0.45 μm cellulose membrane. The particles along with the membrane were placed into 20.0 mL of 0.5 M NaOH solution in a centrifuge tube, mixed on the shaker at 50 rpm for 24 h to recover As(V). The NaOH concentration of 0.5 M was employed following the literature (Cumbal and SenGupta, 2005;

Table 1
Mass Balance Evaluation for Mass Re-equilibrium (MRE) Process.

		Fe_3OMC{Fe_6GAC}				Fe_3OMC{Fe_{23}PAC}				Control[a]		
		Input	Output			Input	Output			Input	Output	
Time (d)		0[b]	1	3	5	0	1	3	5	0	1	5
As amount (μg)	Loaded[c] to or recovered[d] from Fe_3OMC	95.6	51.8	51.5	43.5	95.0	38.6	37.9	37.3	95.5	72.8	69.8
	Recovered[d] from Fe_6GAC or Fe_{23}PAC	N/A[e]	12.4	25.7	38.1	N/A	26.7	44.6	51.0	N/A	N/A	N/A
	In liquid phase[f]	23.1	26.7	31.8	22.3	22.6	14.5	6.95	9.23	23.8	43.4	40.3
	Sum	119	90.9	109	104	118	79.8	89.5	97.5	119	116	110
Add recovered amount from dialysis tubing (= 2.45 μg)			93.3	111	106		82.2	91.9	100		119	113
Recovery percentage (total output/input, %)			78.6	93.8	89.6		69.9	78.1	85.0		100	94.3

[a] Control experiments of Fe_3OMC{Solution II}
[b] 0 d is the time when As is loaded to Fe_3OMC before the MRE process
[c] Amounts loaded to Fe_3OMC are determined with Solution I at MRE 0 d
[d] Recovery amounts are for As in solid phase at MRE 1, 3, 5 d by alkaline extraction
[e] N/A = not applicable
[f] liquid-phase amounts at MRE 0 d are calculated with the 0.5-mL supernatants, and liquid-phase amounts at MRE 1, 3, 5 d are estimated with Solution III by assuming no evaporation. All data are means by duplicate experiments.

Sarkar et al., 2008). After extraction, samples were filtered through a 0.22 μm PES membrane for As analysis to calculate the recovery amount. For $Fe_3OMC\{Fe_{23}PAC\}$ experiment, one more replicate was sacrificed after 5 days' reaction for solid characterizations. For $Fe_3OMC\{Solution\ II\}$ control experiment at 5 day, Fe_3OMC, dialysis tubing, and 0.45 μm cellulose membranes were respectively treated by the same protocol for As(V) recovery.

2.5. Column experiments: demonstration of MRE process

The application feasibility of MRE was tested in column runs using columns packed with Fe_3OMC, Fe_6GAC, and the mixed medium of Fe_3OMC and Fe_6GAC. Specifically, 300-mg solids (0.4-mL bed volume) were packed into 2.5-mL columns (0.9 cm of diameter, 3.9 cm of length, Boca Scientific). For the mixed-medium column, a total of 100-mg Fe_3OMC and 200-mg Fe_6GAC were packed into the column via 4 portions for each, and were added alternatively to help mixing. Glass wool, glass beads, and membrane filters (10-μm, Boca Scientific) were placed into the top and the bottom of each column to support the solid. An upflow fashion was applied and an As(V)-spiked solution was supplied by a peristaltic pump (Masterflex® L/S®, Cole-Parmer). The influent solution was buffered with MOPS (2.0 mM) at pH 6.6, spiked with $NaNO_3$ (50.0 mM), and stored in a Nalgene bottle. Two modes were used, namely, the 10-h-on-14-h-off and non-stop modes. For the former, the empty bed contact times (EBCTs) of columns packed with the mixed medium, Fe_3OMC, and Fe_6GAC were set to 1.00, 0.95, and 0.93 min, respectively; for the latter, EBCTs were 0.95, 0.91, and 0.91 min, respectively. According to the standard method of American Society for Testing and Materials (ASTM, 2014), columns were fed with deionized water for 1 h and then the feedwater was switched to the As(V) test water.

2.6. Chemical analyses

Total As was analyzed by an atomic absorption spectrophotometer with graphite furnace (210 VGP, Buck Scientific) or by an inductively-coupled plasma optical emission spectrometer (iCAP 6500, Thermo-Fisher). Check standards were analyzed regularly, which showed $< 3\%$ relative standard deviation typically. Fe content was determined by a modified 1,10-phenanthroline photometric method as reported previously (Gu et al., 2005).

2.7. Characterizations

Morphology and structure of solids were examined by a transmission electron microscope (TEM, JEOL 1400). The coated Fe forms were evaluated by the high-resolution TEM (HRTEM Tecnai F30, FEI) and fast Fourier transform (FFT) patterns. Energy-filtered TEM (EFTEM) images and electron energy loss spectroscopy (EELS) spectra were obtained by a Quantum Gatan Imaging Filter. The EELS raw spectra, numerically filtered by the second derivative (1.7 eV negative and 4.1 eV positive window width (Botton et al., 1995)) in Gatan Digital Micrograph software (version 3.20), were analyzed as referencing Fe valance to the intensity ratio of Fe L_3 to L_2 electron core-shell transitions (Cosandey et al., 2012; Klie and Browning, 2002). Mineralogy of samples was studied by X-ray diffraction (XRD) (Ultima IV, Rigaku, with Cu K_a radiation at 40 kV, 44 mA, and $\lambda = 1.54$ Å). The oxygen-containing functional groups on carbon surface were investigated by Fourier-transform infrared (FTIR) spectroscopy (Cary 600, Agilent Technologies). Nitrogen adsorption/desorption isotherms at 77 K were conducted on a micropore physisorption analyzer (ASAP 2020Plus HD88, Micromeritics). Brunauer-Emmett-Teller and Barrett–Joyner–Halenda theories were applied to determine specific surface area and pore size distribution, respectively.

As(V) transport for the MRE process was visualized by a focused ion beam scanning electron microscope (FIB-SEM, Scios DualBeam, FEI) equipped with an X-ray energy dispersive spectrometer (EDS, X-Max^N, Oxford Instruments). Valence state of As and Fe for the MRE samples was determined by X-ray photoelectron spectroscopy (XPS, PHI Quantera SXM, PHI-USA) utilizing a scanning X-ray microprobe with an aluminum mono source. All measurements were performed with 26.0 eV pass energy at a 200-μm X-ray spot size. The binding energy was calibrated by referencing the C 1s line at 284.8 eV (Scott et al., 2005) and the spectra were processed with XPSPEAK41 software (see Text S1 for details).

3. Results and Discussion

3.1. Characteristics of Fe-based carbons

To select suitable media in dialysis and column experiments, the solids were first characterized for their porous structures, and then appraised in batch adsorption tests for their ability to adsorb As(V). Fig. S4 showed that the OMC had a highly-ordered porous structure, in contrast to both PAC and GAC. The uniform porous structure of OMC was evidenced by the small-angle XRD pattern of OMC with (100) and (110) reflections (Fig. S5) and the sharp pore size distribution (Fig. S6), in consistency with literature (Meng et al., 2006; Wu et al., 2010). The average particle sizes/ranges for OMC, PAC, GAC were 0.539, 30-42, and 800-1100 μm, respectively (Fig. S7 and Table S1).

After oxidation, the OMC surface gained more functional groups as shown by the FTIR spectra (Fig. S2A), in which the bands at 1629/1639 cm^{-1} may be ascribed to the vibration of C=O bond (quinone groups) (Pakuła et al., 1998; Ramesh and Sampath, 2001) and 3448/3458 cm^{-1} to O-H bond (phenolic hydroxyl groups) (Pradhan and Sandle, 1999; Ramírez et al., 2008). Virgin PAC and GAC had some functional groups. After oxidation (Figs. S2B-C), the bands at 1723-1725 cm^{-1} (the vibration of C=O stretching), together with the bands at 3437-3453 cm^{-1} (hydroxyl groups), could be assigned to carboxyl groups (Moreno-Castilla et al., 1995). The amount of Fe adsorbed on carbon surface correlated with the total amount of hydroxyl-like and carboxyl groups (Pakuła et al., 1998), which explained that the least amount of Fe was coated on the carboxyl-free OMC.

We also analyzed how Fe particles aggregated in the carbon substrate. Some Fe of Fe_3OMC formed separated "islands" (Fig. S8), unlike Fe_6GAC and $Fe_{23}PAC$ with Fe basically covering both outer and inner surfaces (Figs. S9 and S10). The covering explained a sharp decrease of the specific surface areas in comparison with their parent carbons: they were reduced from 877 to 372 and from 650 to 183 m^2/g, respectively, for Fe_6GAC and $Fe_{23}PAC$. The accompanied loss in pore volumes was from 0.530 to 0.230 and 1.02 to 0.186 cm^3/g, respectively. For Fe_3OMC, however, the specific surface area was increased from 554 to 637 m^2/g, possibly because the island-like structure had created more space as the pore volume increased from 0.344 to 0.414 cm^3/g. It is reported that specific surface area is positively related to pore volume (Gniot et al., 2009; Li et al., 2013). Among three parent carbons, the highest pore volume of PAC (1.02 cm^3/g) had allowed the most Fe to aggregate in the porous structure, potentially leading to the largest As(V) adsorption capacity.

Figs. S5A, S6B, and S8A showed the ordered mesoporous channels were maintained after oxidation and Fe-coating. According to raw EELS spectra (Fig. S11), both Fe L and O K edges were detected. And the Fe L_3/L_2 intensity ratios for all three adsorbents were larger than 5.25, suggesting the Fe valence as +3.0 according to literature (Cosandey et al., 2012; Salafranca et al., 2012). Based on the FFT analysis (Figs. S11 and S12), the Fe phase on both Fe_6GAC and $Fe_{23}PAC$ may be hematite as the lattice interpla-

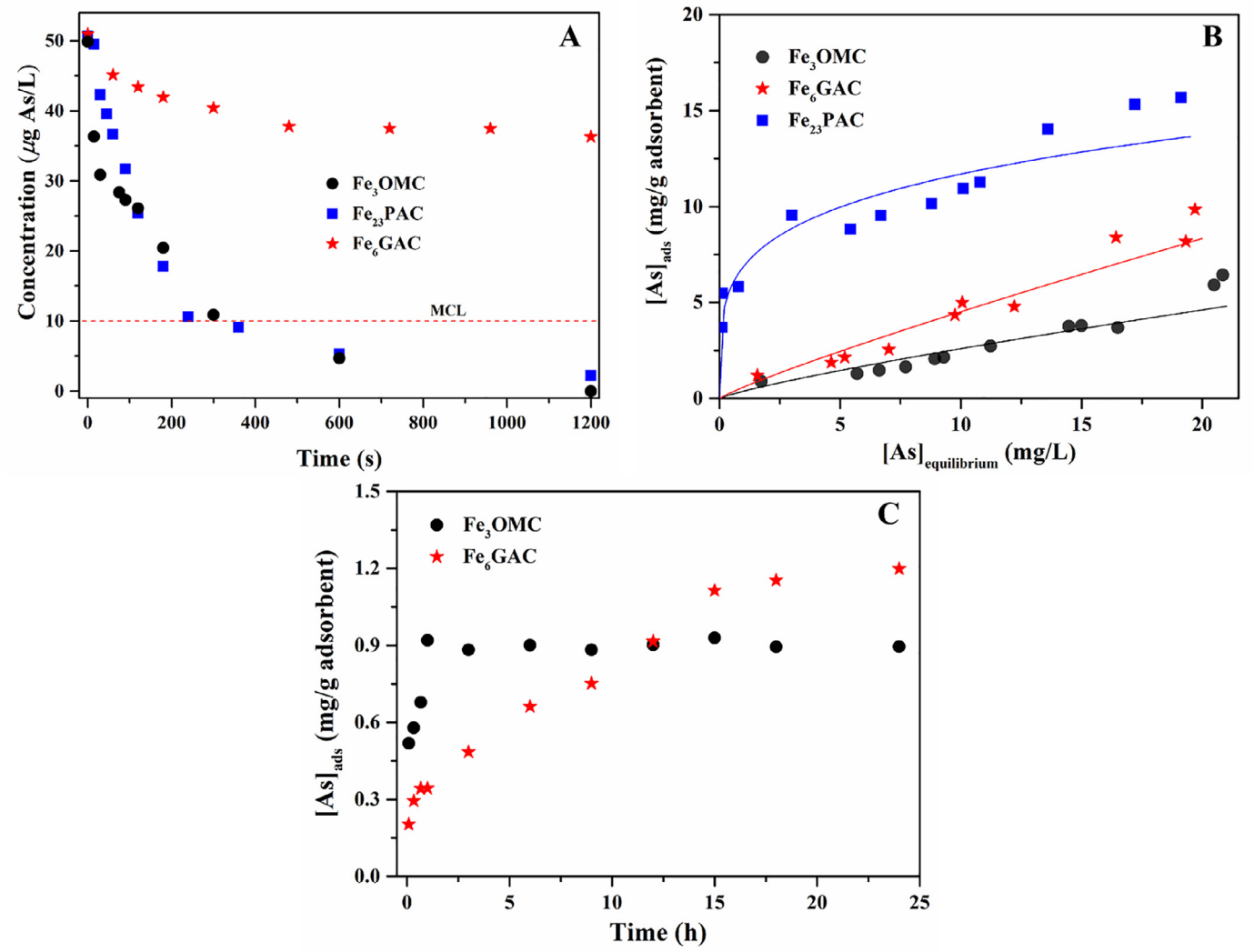

Fig. 2. Adsorption kinetics and isotherms. (A) Kinetics of As(V) adsorption at a solid loading of 1.0 g/L and initial concentrations of 49.9-51.0 μg As/L, monitored at 1200-second time durations; (B) As(V) adsorption isotherms on various Fe-based adsorbents determined using a 24-h equilibrium time, and the corresponding fitting curves based on the Freundlich model (Table S3); (C) Kinetics of As(V) adsorption at a solid loading of 0.5 g/L and initial concentration of 2.17 mg As/L, monitored at 24-hour time durations. Separate vial was used for each time point and MCL means maximum contamination level. Experimental conditions: pH = 6.6, I = 0.05 M, and T = 22°C.

nar distances (see FFT results in Text S2) correspond to planes of hematite based on Joint Committee on Powder Diffraction Standards (JCPDS) Card No. 33-0664, compared to maghemite likely on Fe_3OMC based on JCPDS Card No. 39-1346 (Text S2). Two distinct phases were observed with the same Fe-coating protocol, together with the EFTEM images exhibiting C, O, and Fe distributions (Fig. S13), suggesting that the crystallographic forms of iron oxides may be affected by the surrounding carbon matrices. The formation mechanisms of iron oxides on carbonaceous materials need to be further studied. Nevertheless, we characterized Fe_3OMC with FIB-assisted HRTEM to show the embedment of Fe in the carbon matrix (Fig. S14).

3.2. Batch experiments

Various carbonaceous adsorbents might have very different As(V) uptake rates under otherwise comparable conditions mainly because of their differences in particle size and porous structure. Both Fe_{23}PAC and Fe_3OMC removed As(V) from ~50.0 to below 10.0 μg As/L, the maximum contamination level (Zhang et al., 2017), within less than 300 s, while the As concentration in the system with Fe_6GAC at 300 s remained above the level (Fig. 2A). Given the As(V) uptake rate is "inversely-proportional to the square of particle radius" (Badruzzaman et al., 2004), the slowest uptake rate of Fe_6GAC may be partially due to the largest grain size of the GAC that is 800-1100 μm. The well-documented "highway" mass transfer effects (Korenblit et al., 2010), as represented by rapid uptake of ordered mesoporous materials, were observed for the faster adsorption on Fe_3OMC than on Fe_{23}PAC when time < 100 s. With a much higher Fe content for the latter, however, the adsorbed amount caught up with the former at 120 s; the similar trend was observed previously (Gu et al., 2007). According to the pore size distribution (Figs. S6C-D), the existence of larger pores (> 5 nm) for Fe_{23}PAC and the highest fraction of small pores (< 2.5 nm) for Fe_6GAC corresponded to the fastest and the slowest adsorption rate, which was consistent with other studies for a positive correlation between fast mass transfer and large porosity (Badruzzaman et al., 2004; Hristovski et al., 2008). Fitting kinetic data of Fe_{23}PAC, Fe_3OMC, and Fe_6GAC with the intraparticle diffusion model (Kim et al., 2004; Yu et al., 2009) gave the rate constants of 2.24, 2.12, and 0.633 $\mu g\ g^{-1}\ s^{-0.5}$, respectively (see details in Table S2), suggesting that the rate-limiting step was intraparticle diffusion.

The control experiments showed that parent carbons cannot adsorb much As(V), that is, ~0.091, ~0.174, and ~0.347 mg As/g for OMC, PAC, and GAC, respectively. The adsorption capacities mea-

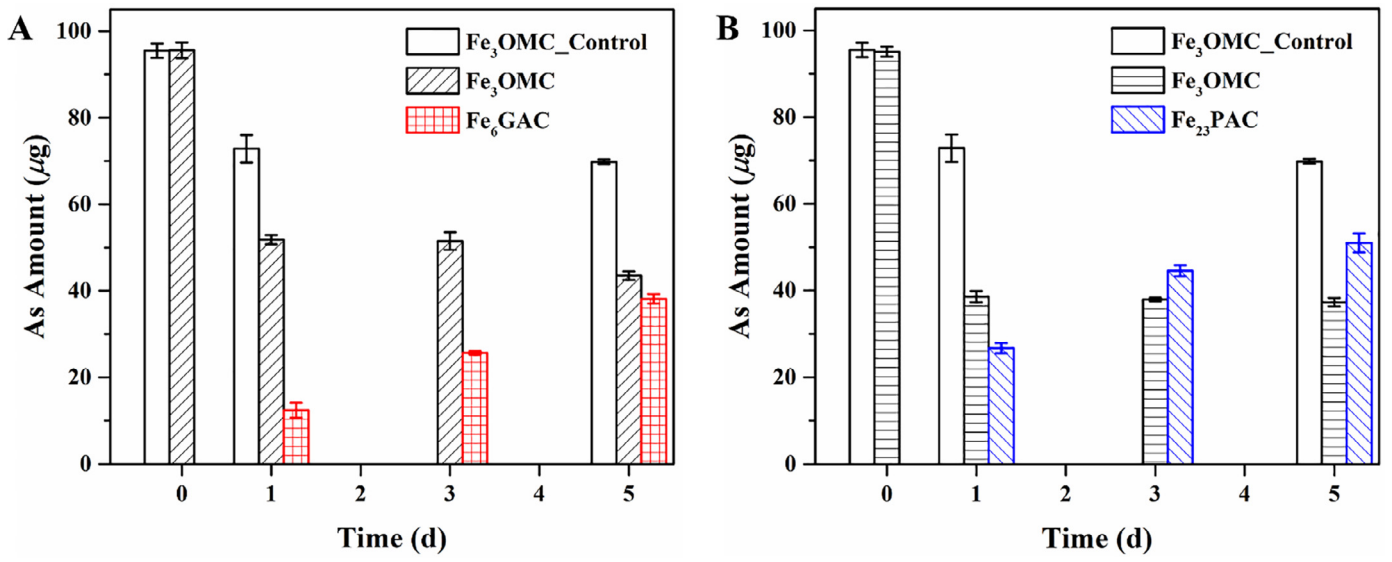

Fig. 3. The As amounts (unit in μg) in solid phase after 1, 3, 5 d MRE reactions for (A) $Fe_3OMC\{Fe_6GAC\}$ and (B) $Fe_3OMC\{Fe_{23}PAC\}$ experiments. $Fe_3OMC\{Solution\ II\}$ experiments are the control. Amounts at MRE 0 d correspond to As amounts loaded to Fe_3OMC. Data are expressed as mean ± range by duplicate tests with error bars for ranges. As amounts in liquid phase, estimated with Solution III, are seen in Table 1. Solutions I, II, and III are defined in section 2.4. The mass ratio of Fe_3OMC to Fe_6GAC (or $Fe_{23}PAC$) is 1 to 2. Experimental conditions: pH = 6.6, I = 0.05 M, and T = 22°C.

sured for Fe_3OMC, Fe_6GAC, and $Fe_{23}PAC$ (Fig. 2B) were 6.44, 10.4, and 15.7 mg As/g, respectively, in accordance with the increasing order of Fe contents. Despite unsatisfactory regression coefficients of the Freundlich fits (R^2 = 0.880-0.931, Table S3), the model described the results better than the Langmuir model (data not shown).

Knowing Fe_6GAC adsorbed more As(V) at equilibrium of 24 h but with a slower uptake rate than Fe_3OMC, we designed the 24-hour kinetic tests. Fig. 2C shows the adsorption plateau reached in 1 h for Fe_3OMC and 18 h for Fe_6GAC, and a crossover was observed at 12 h. Afterwards, we evaluated the MRE process in dialysis experiments and assessed the application feasibility with the mixed medium in column tests.

3.3. As(V) transport in MRE process

The pseudo-equilibrium model aforementioned could be represented by Eqs. 3 and 4 (Morel and Hering, 1993):

$$M + P \underset{k_{-1}}{\overset{k_1}{\rightleftarrows}} MP; \quad K_{MP} \tag{3}$$

$$M + Q \underset{k_{-2}}{\overset{k_2}{\rightleftarrows}} MQ; \quad K_{MQ} \tag{4}$$

where k_1, k_{-1}, k_2, k_{-2} are the rate constants (s^{-1}), K_{MP} and K_{MQ} are the complexation constants, M represents a metal, and P and Q are two competing ligands. Assumptions were made (Morel and Hering, 1993): i) ideally, reactions (3) and (4) obeyed pseudo-first-order kinetics with the rate constants $k_1^* \gg k_2^* (k_1^* = k_1 \times [P], k_2^* = k_2 \times [Q])$; ii) the weaker ligand P ($K_{MP} \ll K_{MQ}$) was more abundant at the initial condition, i.e., $[P]_0 \gg [Q]_0$; and iii) $[Q]_0 \gg [M]_0$. The model revealed the pseudo-equilibrium was reached quickly between species M and MP with $[MP] \gg [MQ]$ during this time interval. But the final equilibrium was re-established later, resulting in $[MQ] > [MP]$ due to the competition for the surface sites. Insights from the pseudo-equilibrium model allowed us to evaluate the MRE process in which As(V) initially in a pseudo-equilibrium with the fast-adsorbing Fe_3OMC is supposed to redistribute with time and eventually reach the true equilibrium with both media.

The observation of the As(V) transport from Fe_3OMC to Fe_6GAC, or $Fe_{23}PAC$, clearly established the MRE process moving towards the "true" equilibrium (Fig. 3). Setting up dialysis tubing ("{}") allowed As(V), rather than adsorbents confined in, to diffuse through. At the beginning, the As amounts loaded to Fe_3OMC were 95.5, 95.6, and 95.0 μg for $Fe_3OMC\{Solution\ II\}$ (the control), $Fe_3OMC\{Fe_6GAC\}$, and $Fe_3OMC\{Fe_{23}PAC\}$ experiments, respectively. For $Fe_3OMC\{Solution\ II\}$, the solid-phase As amounts at MRE 1 and 5 d, recovered from Fe_3OMC by alkaline extraction, were 72.8 and 69.8 μg, respectively. In comparison, adding Fe_6GAC to the system induced more As release from Fe_3OMC, as evidenced by smaller recovery amounts of 51.8 and 43.5 μg from Fe_3OMC at 1 and 5 d, respectively, and by As accumulation on Fe_6GAC from 12.4 μg at 1 d to 38.1 μg at 5 d (Fig. 3A). When $Fe_{23}PAC$ with the highest adsorption capacity was introduced, the extractable amount from Fe_3OMC was the smallest (37.3 μg at 5 d), with the highest amount of 51.0 μg concurrently accumulating on $Fe_{23}PAC$ at 5 d (Fig. 3B). Given the accumulating amounts at 5 d for Fe_6GAC and $Fe_{23}PAC$ were clearly higher than the liquid-phase amounts at 0 d (23.1 and 22.6 μg, respectively), there must be As(V) transporting away from the As-loaded Fe_3OMCs, confirming the MRE process.

The high As amounts recoverable from both Fe_6GAC and $Fe_{23}PAC$ were also due to the decreased liquid-phase amounts from 1 to 5 d (Fig. S15). Overall mass balance calculations (Table 1) quantified the mass transfer of As(V) in the MRE process. The mass recoveries were >78.0% for most systems. The <100% recoveries could be attributed to the loss of particles during operation and the incomplete recovery of As from spent Fe-based carbons. As reported, 0.5 M NaOH cannot attain 100% As recovery (Cumbal and SenGupta, 2005; Sarkar et al., 2008). In addition, the amounts of As adsorbed onto the dialysis tubings and cellulose membranes were measured to be 2.45 and 1.67 μg at MRE 5 d, respectively, indicating that while both adsorbed trace amounts of As, the percentage was only 2.05% and 1.40% of the inputs.

To examine As(V) transport in the MRE process, we conducted extensive analyses on the freeze-dried solids from $Fe_3OMC\{Fe_{23}PAC\}$ experiments with XPS and HRTEM-FFT. In terms of As 3*d* spectra (Figs. S16A, C, E), the peaks centered at 45.2-

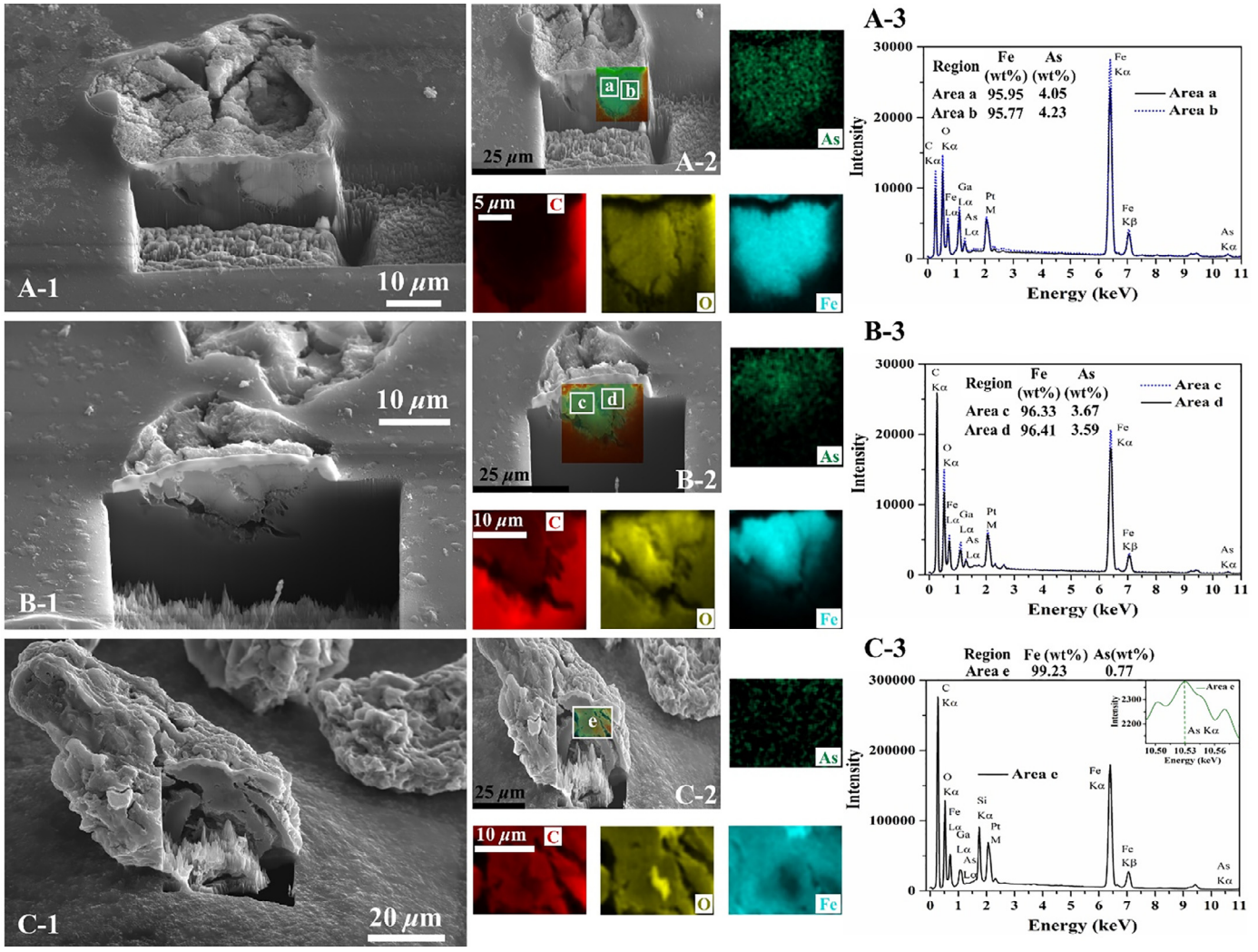

Fig. 4. SEM images (A-1, B-1, C-1) and elemental mappings (A-2, B-2, C-2 for C, O, Fe, and As) of ablated grains by FIB, with EDS spectra (A-3, B-3, C-3) for elemental analysis. The EDS spectra are based on five different regions (Areas a-e), marked with white squares in mappings. All reacted solids are collected from Fe_3OMC{$Fe_{23}PAC$} experiments. Fe_3OMC samples at MRE 0 d (A-1, A-2, A-3) and at MRE 5d (B-1, B-2, B-3) are analyzed. One $Fe_{23}PAC$ sample at MRE 5d (C-1, C-2, C-3) is analyzed with the inset of C-3 showing As Kα spectrum for Area e. Ga and Pt are introduced by the FIB, while Si is from the parent carbon according to the manufacturer.

45.7 eV were associated with the adsorbed As(V) (Nesbitt and Reinke, 1999; Prucek et al., 2013; Zhang et al., 2017). Together with the contributions from Fe(III) for Fe 2*p* spectra, i.e., Fe $2p_{3/2}$ peaks located at 711.4 eV (Bonnissel-Gissinger et al., 1998; McIntyre and Zetaruk, 1977) (Figs. S16B, D, F), we found no redox reactions between As(V) and the coated iron oxides in carbon matrices. HRTEM-FFT microanalysis suggested that iron-oxide crystallinity may not change after reactions (Fig. S17), as the Fe phases of Fe_3OMC and $Fe_{23}PAC$ were still maghemite and hematite, respectively.

Both inner and outer surfaces of reacted grains from Fe_3OMC{$Fe_{23}PAC$} experiments were observed with FIB technique. On the mappings of the cross section, it clearly showed Fe being embedded in the carbon substrate (Fig. 4). For a comprehensive visualization of As(V) sequestration, 31 regions, from Areas a to ae (Fig. 4 and Figs. S18-S20, see summary in Table S4), were selected for elemental analysis, based on EDS spectra. Fe and As distributions were correlated well with the reacted Fe_3OMC grains (Figs. 4A-2 and 4B-2), while a much weaker As mapping was observed for the reacted $Fe_{23}PAC$ grain (Fig. 4C-2). The relative As weight percentage on the inner surface of Fe_3OMC at 0 d (Areas a, b in Fig. 4A-2 and f, g in Fig. S18A) and 5 d (Areas c, d in Fig. 4B-2 and h, i in Fig. S18B) was 3.72 ± 0.49 and 2.92 ± 0.83 wt. % (± standard deviation), respectively, which suggested that not much As(V) transported away from the interior. Hence, the smaller As recovery amounts from Fe_3OMC could be ascribed to more As(V) release from the exterior surface: corresponding As weight percentage at 0 d (Areas j, k, l, m, n in Figs. S19A-B) and 5 d (Areas o, p, q, r in Figs. S19C-D) was 8.90 ± 2.44 and 4.32 ± 0.89 wt. %, respectively. For $Fe_{23}PAC$, though As was occasionally not detected on two areas, the broad weight-percentage distributions from 0.43 to 5.75 wt. % based on another eleven areas illustrated the sequestration (Areas s to ae in Fig. S20). The 0.77 wt. % of As on the inner surface (Fig. 4C-3) implied very little As(V) can diffuse to the internal regions of reacted $Fe_{23}PAC$ grains.

As(V) adsorption rate is normally much faster than desorption rate (Grossl et al., 1997; Yang et al., 2012), and only a small fraction of adsorbed As(V) releases at (near)neutral pH, possibly due to the high activation barriers for As(V) desorption (Farrell and Chaudhary, 2013) and/or slow mass transfer effects out of micropores of iron oxides (Cornell and Schwertmann, 2003). Meanwhile, As(V) desorption generally underwent dual stages. Outer-sphere complexation, observed on hematite-As(V), may account for the faster release at the first stage (Catalano et al., 2008) because these complexes were formed by a combination of electrostatic attraction, hydrogen bonding, and configurationally interfacial-water stabiliza-

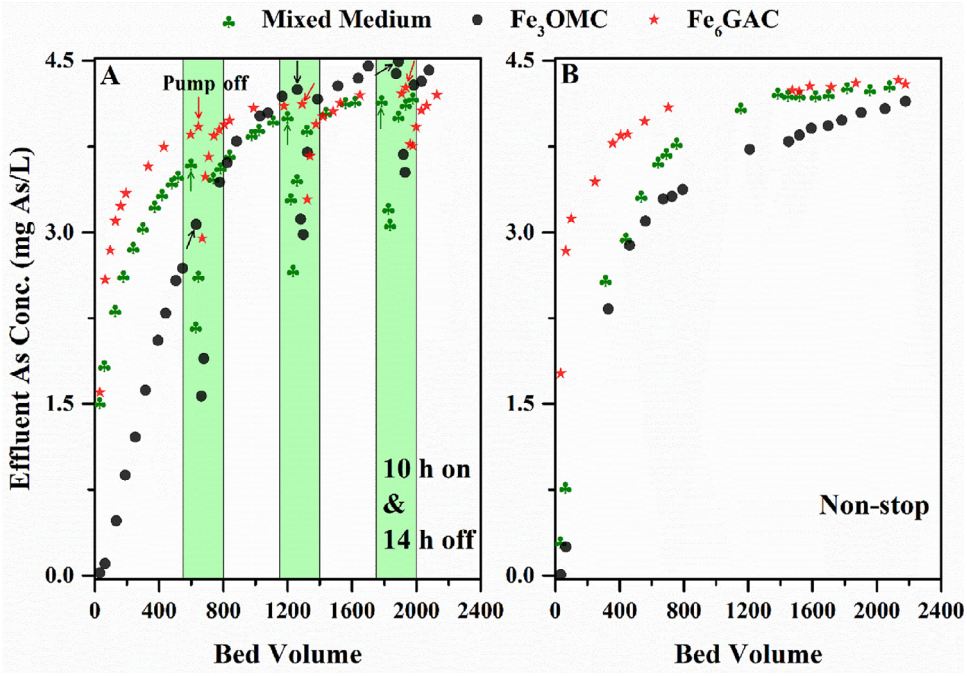

Fig. 5. As(V) breakthrough curves. (A) Columns run on a 10-h-on and 14-h-off mode every day and EBCTs of columns packed with the mixed medium, Fe_3OMC, and Fe_6GAC are 1.00, 0.95, and 0.93 min, respectively. Pump shutdown periods (14-h off cycles) are indicated by arrows in the green shaded areas. (B) Columns run on a non-stop mode and EBCTs with the mixed medium, Fe_3OMC, and Fe_6GAC are 0.95, 0.91, and 0.91 min, respectively. Column run conditions: influent concentration = 4.64 mg As/L, pH = 6.6, I = 0.05 M, and T = 22°C.

tion (Catalano et al., 2008). We assumed that some outer-sphere As(V) surface complexes were formed on the coated maghemite of Fe_3OMC. Then, the release of As(V) in the outer-sphere complexes could be partially responsible for the sharp drop of solid-phase amounts from MRE 0 to 1 d in Fe_3OMC{Solution II} control experiments (Fig. 3). It was followed by the apparent level-off from 1 to 5 d at the second stage.

In general, the coordination bond cleavage of inner-sphere complexes would hinder further release of As(V) at near-neutral pH Farrell and Chaudhary, 2013). Even in the presence of 6 mM phosphate solution at pH 6, the desorbed fraction of As(V) from goethite in ~100 h was almost the same as the fraction in ~700 h, and the bonding mechanism of inner-sphere complexes did not change after one week (O'Reilly et al., 2001). However, after adding the competing adsorbent to the system, much more was desorbed from Fe_3OMC than the control (Fig. 3). Since the As(V) release from the inside of As-loaded Fe_3OMC contributed to the MRE in a minor way (Fig. 4), we assumed the inner-sphere complexes on the outer surface of Fe_3OMC could be more likely involved in the MRE-based As(V) desorption. Meanwhile, we observed that the larger the adsorption capacity of the competing adsorbent, the more As(V) release from Fe_3OMC. This can be explained by Eqs. (1) and ((2), as a stronger adsorbent of $Fe_{23}PAC$, or $\equiv M''$ in Eq. (2), could better compete for As(V) with Fe_3OMC, or $\equiv M'$ in Eq. (1), thus favoring the forward reaction in Eq. (2). In summary, we demonstrated the feasibility of using the MRE process for As(V) transport from the spent adsorbent to a virgin one at this stage.

3.4. Column studies

We performed column tests with the mixed medium containing both Fe_3OMC and Fe_6GAC at a mass ratio of 1:2, and with the single medium of Fe_3OMC or Fe_6GAC. We ran column tests on a 10-h-on and 14-h-off mode to potentially match diurnal variability in a household (Fig. 5A), in comparison with a continuous mode (Fig. 5B). Such on-off mode of operation could enhance As(V) uptake when the flow was restarted (Westerhoff et al., 2005). We employed a high As influent concentration (4.64 mg As/L) to assess the potential of engineering MRE process. The results indicated that: 1) generally, the effluent As concentrations increased with time for all three columns; 2) the Fe_3OMC column removed As(V) most effectively in the first 800 bed volumes (BVs). After each 14-h-off period, there was an improved As(V) removal for all as indicated by sharp drops in As concentration; for example, the concentration dropped by almost half in the Fe_3OMC column (Fig. 5A). This drop in the Fe_3OMC column was, however, very brief, which could be rationalized by the lack of sufficient adsorption sites on Fe_3OMC under the high influent concentration. In the Fe_6GAC column with a large capacity but slow kinetics for As(V), the performance for As(V) removal was the worst in the first 1000 BVs but outperformed the Fe_3OMC column afterwards (Fig. 5A) because of the near exhaustion of Fe_3OMC.

In contrast, when the mixed medium was used, while the efficiency for As(V) removal was not as good as that of the pure Fe_3OMC column in the first 800 BVs, the mixed-medium column outperformed the Fe_3OMC one afterwards, as indicated by the crossover of As(V) breakthrough curves at around 800 BVs (Fig. 5A). That is, in the mixed-medium column, Fe_3OMC can adsorb As(V) faster than Fe_6GAC on a per-gram-medium basis (see Fig. 2C for reference), and then the MRE can kick in that could moderately regenerate Fe_3OMC *in situ* in the off-pump cycles, eventually leading to a lower effluent As(V) level. This suggested that some As(V) loaded on Fe_3OMC could diffuse to Fe_6GAC during the idle period. When compared with the pure Fe_6GAC column, the mixed-medium column had a better performance before 800 BVs possibly due to faster kinetics of Fe_3OMC.

The column interruption tests and corresponding solid-phase concentration gradients (dq/dr) have been applied to understand contaminant adsorption, as illustrated by Fig. 6. When intraparticle diffusion is a rate-limiting step, like this study, the solid-phase concentration gradient of a single particle that governs the overall uptake rate tends to level out during the interruption (Li and SenGupta, 2000; SenGupta, 2017). Right after, a larger driving force, represented by a greater dq/dr due to the interrup-

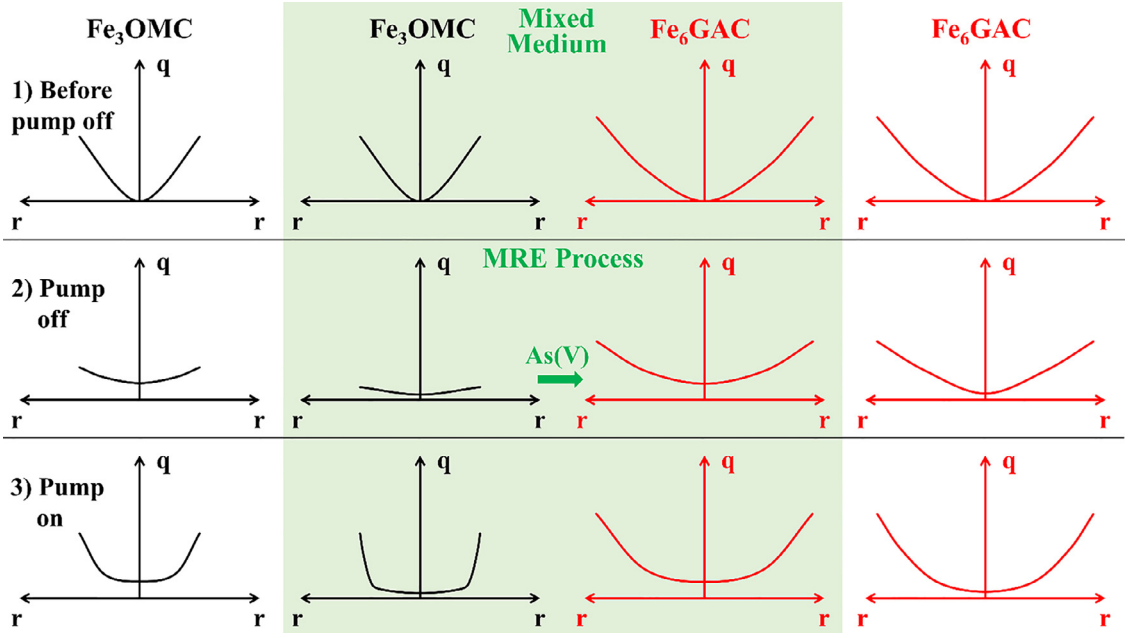

Fig. 6. Proposed solid-phase As(V) concentration profile of a single particle for columns running with the on-off pump cycling mode. The solid-phase concentration (q) is displayed as a function of particle radius (r) and the basic concept is adapted from SenGupta, 2017. From left to right are illustrations of columns packed with Fe_3OMC, mixed medium (the green shaded area), and Fe_6GAC. For the mixed medium, separate concentration profiles of Fe_3OMC and Fe_6GAC are shown. Three stages are illustrated: before pump shutdown at stage 1, the concentration profiles of Fe_3OMC and Fe_6GAC are the same for the mixed-medium and single-medium columns; during pump-off period at stage 2, As(V) diffuses from Fe_3OMC to Fe_6GAC in the mixed media.

tion, can improve the uptake and drop the effluent solute level (Li and SenGupta, 2000; SenGupta, 2017). The solid-phase As(V) concentration profiles for Fe_3OMC and Fe_6GAC could be similarly conceptualized with dq/dr changing over an on-off pump cycle (Fig. 6). In terms of the mixed-medium column (the green shaded area), adsorbed As(V) can diffuse and redistribute between Fe_3OMC and Fe_6GAC by the MRE during interruption, thus further leveling off the dq/dr of Fe_3OMC. The situation is equivalent to *in situ* regeneration of Fe_3OMC, via intraparticle diffusion of the desorbed As(V) from Fe_3OMC into Fe_6GAC. Upon restarting the flow, the regenerated Fe_3OMC with a much enhanced dq/dr could adsorb As more quickly so resulting in a rapid decrease of effluent concentration.

For practical application, this on-and-off mode of operation would be consistent with the demand of most households. In the continuous mode of operation (Fig. 5B) where there was not enough time for MRE, the As(V) removal effectiveness in the columns followed the order of Fe_3OMC > the mixed medium > Fe_6GAC, as expected. When GAC is doped with maghemite nanoparticles, magnetically separating the spent GAC and then replenishing a new portion would be another possibility. Taken together, the column results showed the possibility of engineering an MRE process for the enhanced As(V) removal upon the on-off pump cycling operation.

4. Conclusions

The batch tests and elemental mappings of this study showed that the desorption of As(V) from an adsorbent can be enhanced by another in close proximity. When As(V) release is well-controlled, a binary-adsorbent system could be engineered by mixing one fast-uptake adsorbent with the other with a higher adsorption capacity in column runs. The crossover of As(V) breakthrough curves (Fig. 5A) suggested that the solid-phase concentrations were altered due to potential redistribution of As(V) during pump-off periods. For any adsorption columns operated for households, rapid As(V) uptake is essential to cope with a short EBCT, e.g., 32 seconds (Möller et al., 2009). The shorter the EBCT, the sooner the breakthrough, as in general, the progression of the mass transfer zone is irreversible with water flow. While for those time periods when the household-scale filtration column is on standby, the As(V) re-equilibrium might re-shape the mass transfer zone, as the adsorbent with a higher capacity but slower kinetics could regenerate the fast-adsorbing one *in situ*. The MRE phenomenon examined here may also be applicable to the removal of other contaminants such as phosphate, due to similar interactions for adsorbing it on iron-based materials.

Last but not least, since cost-benefit is not studied, the efficacy of MRE process in practice needs to be further analyzed, especially when effluent concentrations are lower than those of this study. Life cycle assessment of the pros and cons of MRE-based *in-situ* adsorbent regeneration will be important in comparing the binary-adsorbent system with the conventional process configuration.

Declaration of Competing interest

The authors declare that they have no known competing financial interests or personal relationships that could have appeared to influence the work reported in this paper.

Acknowledgements

This work was partially supported by Amway Corp. (#00043734) and the University of Missouri (MU) Electron Microscopy Core Facility *via* “Excellence in Electron Microscopy” award. The support by Dr. Zhenxiao Cai at Amway is greatly appreciated. Drs. Qingsong Yu, Jian Lin, and Chi Zhang (MU) are thanked for helping us with FTIR facility, tubular furnace, and XPS spectrum analysis, respectively. Cabot Corp. and Evoqua Water Technologies are thanked for providing us with ACs. Help from Dr. Joseph J. Pignatello and assistance with As analysis from Mr. Craig Musante (The Connecticut Agricultural Experiment Station) are acknowledged. Comments from anonymous reviewers are of great use to the quality improvement of this study.

Supplementary materials

Supplementary material associated with this article can be found, in the online version, at doi:10.1016/j.watres.2020.116676.

References

ASTM, 2014. D6586-03, Standard Practice for the Prediction of Contaminant Adsorption On GAC In Aqueous Systems Using Rapid Small-Scale Column Tests, American Society for Testing and Materials (ASTM), West Conshohocken, PA.

Badruzzaman, M., Westerhoff, P., Knappe, D.R.U., 2004. Intraparticle diffusion and adsorption of arsenate onto granular ferric hydroxide (GFH). Water Res 38 (18), 4002–4012.

Baikousi, M., Georgiou, Y., Daikopoulos, C., Bourlinos, A.B., Filip, J., Zbořil, R., Deligiannakis, Y., Karakassides, M.A., 2015. Synthesis and characterization of robust zero valent iron/mesoporous carbon composites and their applications in arsenic removal. Carbon 93, 636–647.

Bakshi, S., Banik, C., Rathke, S.J., Laird, D.A., 2018. Arsenic sorption on zero-valent iron-biochar complexes. Water Res 137, 153–163.

Bonnissel-Gissinger, P., Alnot, M., Ehrhardt, J.-J., Behra, P., 1998. Surface Oxidation of Pyrite as a Function of pH. Environ. Sci. Technol. 32 (19), 2839–2845.

Botton, G.A., Appel, C.C., Horsewell, A., Stobbs, W.M., 1995. Quantification of the EELS near-edge structures to study Mn doping in oxides. J Microsc 180 (3), 211–216.

Catalano, J.G., Park, C., Fenter, P., Zhang, Z., 2008. Simultaneous inner- and outer–sphere arsenate adsorption on corundum and hematite. Geochim. Cosmochim. Acta 72 (8), 1986–2004.

Chen, W., Parette, R., Zou, J., Cannon, F.S., Dempsey, B.A., 2007. Arsenic removal by iron-modified activated carbon. Water Res 41 (9), 1851–1858.

Cornell, R.M., Schwertmann, U., 2003. The Iron Oxides: Structure, Properties, Reactions, Occurrences and Uses. Wiley, Weinheim, pp. 253–296.

Cosandey, F., Su, D., Sina, M., Pereira, N., Amatucci, G.G., 2012. Fe valence determination and Li elemental distribution in lithiated $FeO_{0.7}F_{1.3}$/C nanocomposite battery materials by electron energy loss spectroscopy (EELS). Micron 43 (1), 22–29.

Couture, R.M., Rose, J., Kumar, N., Mitchell, K., Wallschläger, D., Van Cappellen, P., 2013. Sorption of Arsenite, Arsenate, and Thioarsenates to Iron Oxides and Iron Sulfides: A Kinetic and Spectroscopic Investigation. Environ. Sci. Technol. 47 (11), 5652–5659.

Cui, J., Shi, J., Jiang, G., Jing, C., 2013. Arsenic Levels and Speciation from Ingestion Exposures to Biomarkers in Shanxi, China: Implications for Human Health. Environ. Sci. Technol. 47 (10), 5419–5424.

Cumbal, L., SenGupta, A.K., 2005. Arsenic Removal Using Polymer-Supported Hydrated Iron(III) Oxide Nanoparticles: Role of Donnan Membrane Effect. Environ. Sci. Technol. 39 (17), 6508–6515.

Farrell, J., Chaudhary, B.K., 2013. Understanding Arsenate Reaction Kinetics with Ferric Hydroxides. Environ. Sci. Technol. 47 (15), 8342–8347.

Fendorf, S., Eick, M.J., Grossl, P., Sparks, D.L., 1997. Arsenate and Chromate Retention Mechanisms on Goethite. 1. Surface Structure. Environ. Sci. Technol. 31 (2), 315–320.

Gniot, I., Kirszensztejn, P., Kozłowski, M., 2009. Oxidative dehydrogenation of isobutane using modified activated carbons as catalysts. Applied Catalysis A: General 362 (1–2), 67–74.

Grossl, P.R., Eick, M., Sparks, D.L., Goldberg, S., Ainsworth, C.C., 1997. Arsenate and Chromate Retention Mechanisms on Goethite. 2. Kinetic Evaluation Using a Pressure-Jump Relaxation Technique. Environ. Sci. Technol. 31 (2), 321–326.

Gu, Z., Deng, B., Yang, J., 2007. Synthesis and evaluation of iron-containing ordered mesoporous carbon (FeOMC) for arsenic adsorption. Microporous Mesoporous Mater 102 (1), 265–273.

Gu, Z., Fang, J., Deng, B., 2005. Preparation and Evaluation of GAC-Based Iron–Containing Adsorbents for Arsenic Removal. Environ. Sci. Technol. 39 (10), 3833–3843.

Hristovski, K.D., Westerhoff, P.K., Crittenden, J.C., Olson, L.W., 2008. Arsenate Removal by Nanostructured ZrO_2 Spheres. Environ. Sci. Technol. 42 (10), 3786–3790.

Hu, X., Ding, Z., Zimmerman, A.R., Wang, S., Gao, B., 2015. Batch and column sorption of arsenic onto iron-impregnated biochar synthesized through hydrolysis. Water Res 68, 206–216.

Kalaruban, M., Loganathan, P., Nguyen, T.V., Nur, T., Hasan Johir, M.A., Nguyen, T.H., Trinh, M.V., Vigneswaran, S., 2019. Iron-impregnated granular activated carbon for arsenic removal: Application to practical column filters. J. Environ. Manage. 239, 235–243.

Kim, Y., Kim, C., Choi, I., Rengaraj, S., Yi, J., 2004. Arsenic Removal Using Mesoporous Alumina Prepared via a Templating Method. Environ. Sci. Technol. 38 (3), 924–931.

Klie, R.F., Browning, N.D., 2002. Characterization of oxygen ordering in (La, Sr)$FeO_{3-\delta}$ by atomic resolution Z-contrast imaging and electron energy-loss spectroscopy. J. Electron Microsc. 51 (suppl_1), S59–S66.

Korenblit, Y., Rose, M., Kockrick, E., Borchardt, L., Kvit, A., Kaskel, S., Yushin, G., 2010. High-Rate Electrochemical Capacitors Based on Ordered Mesoporous Silicon Carbide-Derived Carbon. ACS Nano 4 (3), 1337–1344.

Li, N., Zhu, J., Ma, X., Zha, Q., Song, C., 2013. Tailoring of surface oxygen-containing functional groups and their effect on adsorptive denitrogenation of liquid hydrocarbons over activated carbon. AlChE J 59 (4), 1236–1244.

Li, P., SenGupta, A.K., 2000. Intraparticle Diffusion during Selective Sorption of Trace Contaminants: The Effect of Gel versus Macroporous Morphology. Environ. Sci. Technol. 34 (24), 5193–5200.

McGrory, E.R., Brown, C., Bargary, N., Williams, N.H., Mannix, A., Zhang, C., Henry, T., Daly, E., Nicholas, S., Petrunic, B.M., Lee, M., Morrison, L., 2017. Arsenic contamination of drinking water in Ireland: A spatial analysis of occurrence and potential risk. Sci. Total Environ. 579 (Supplement C), 1863–1875.

McIntyre, N.S., Zetaruk, D.G., 1977. X-ray photoelectron spectroscopic studies of iron oxides. Anal. Chem. 49 (11), 1521–1529.

Meng, Y., Gu, D., Zhang, F., Shi, Y., Cheng, L., Feng, D., Wu, Z., Chen, Z., Wan, Y., Stein, A., 2006. A family of highly ordered mesoporous polymer resin and carbon structures from organic-organic self-assembly. Chem. Mater. 18 (18), 4447–4464.

Mertens, J., Rose, J., Wehrli, B., Furrer, G., 2016. Arsenate uptake by Al nanoclusters and other Al-based sorbents during water treatment. Water Res 88, 844–851.

Middleton, D.R.S., Watts, M.J., Hamilton, E.M., Ander, E.L., Close, R.M., Exley, K.S., Crabbe, H., Leonardi, G.S., Fletcher, T., Polya, D.A., 2016. Urinary arsenic profiles reveal exposures to inorganic arsenic from private drinking water supplies in Cornwall. UK. Sci Rep 6, 25656.

Möller, T., Sylvester, P., Shepard, D., Morassi, E., 2009. Arsenic in groundwater in New England — point-of-entry and point-of-use treatment of private wells. Desalination 243 (1), 293–304.

Moraga, B., Toledo, L., Jelínek, L., Yañez, J., Rivas, B.L., Urbano, B.F., 2019. Copolymer–hydrous zirconium oxide hybrid microspheres for arsenic sorption. Water Res 166, 115044.

Morel, F., Hering, J.G., 1993. Principles and Applications of Aquatic Chemistry. Wiley, New York, pp. 141–146.

Moreno-Castilla, C., Ferro-Garcia, M.A., Joly, J.P., Bautista-Toledo, I., Carrasco–Marin, F., Rivera-Utrilla, J., 1995. Activated Carbon Surface Modifications by Nitric Acid, Hydrogen Peroxide, and Ammonium Peroxydisulfate Treatments. Langmuir 11 (11), 4386–4392.

Nesbitt, H.W., Reinke, M., 1999. Properties of As and S at NiAs, NiS, and $Fe_{1-X}S$ surfaces, and reactivity of niccolite in air and water. Am. Mineral. 84 (4), 639–649.

Neumann, A., Kaegi, R., Voegelin, A., Hussam, A., Munir, A.K.M., Hug, S.J., 2013. Arsenic Removal with Composite Iron Matrix Filters in Bangladesh: A Field and Laboratory Study. Environ. Sci. Technol. 47 (9), 4544–4554.

O'Reilly, S.E., Strawn, D.G., Sparks, D.L., 2001. Residence time effects on arsenate adsorption/desorption mechanisms on goethite. Soil Sci Soc Am J 65 (1), 67–77.

Pakuła, M., Biniak, S., Świątkowski, A., 1998. Chemical and Electrochemical Studies of Interactions between Iron(III) Ions and an Activated Carbon Surface. Langmuir 14 (11), 3082–3089.

Pérez-Vidal, A., Diaz-Gómez, J., Castellanos-Rozo, J., Usaquen-Perilla, O.L., 2016. Long-term evaluation of the performance of four point-of-use water filters. Water Res 98, 176–182.

Peter, K.T., Johns, A.J., Myung, N.V., Cwiertny, D.M., 2017. Functionalized polymer–iron oxide hybrid nanofibers: Electrospun filtration devices for metal oxyanion removal. Water Res 117, 207–217.

Pradhan, B.K., Sandle, N.K., 1999. Effect of different oxidizing agent treatments on the surface properties of activated carbons. Carbon 37 (8), 1323–1332.

Prucek, R., Tuček, J., Kolařík, J., Filip, J., Marušák, Z., Sharma, V.K., Zbořil, R., 2013. Ferrate(VI)-Induced Arsenite and Arsenate Removal by In Situ Structural Incorporation into Magnetic Iron(III) Oxide Nanoparticles. Environ. Sci. Technol. 47 (7), 3283–3292.

Ramesh, P., Sampath, S., 2001. Electrochemical and spectroscopic characterization of quinone functionalized exfoliated graphite. Analyst 126 (11), 1872–1877.

Ramírez, C., Rico, M., Torres, A., Barral, L., López, J., Montero, B., 2008. Epoxy/POSS organic–inorganic hybrids: ATR-FTIR and DSC studies. Eur. Polym. J. 44 (10), 3035–3045.

Ray, J.R., Shabtai, I.A., Teixidó, M., Mishael, Y.G., Sedlak, D.L., 2019. Polymer-clay composite geomedia for sorptive removal of trace organic compounds and metals in urban stormwater. Water Res 157, 454–462.

Salafranca, J., Gazquez, J., Pérez, N., Labarta, A., Pantelides, S.T., Pennycook, S.J., Batlle, X., Varela, M., 2012. Surfactant Organic Molecules Restore Magnetism in Metal-Oxide Nanoparticle Surfaces. Nano Lett 12 (5), 2499–2503.

Sankar, M.U., Aigal, S., Maliyekkal, S.M., Chaudhary, A., Anshup, Kumar, A.A., Chaudhari, K., Pradeep, T., 2013. Biopolymer-reinforced synthetic granular nanocomposites for affordable point-of-use water purification. Proc. Natl. Acad. Sci. U.S.A. 110 (21), 8459–8464.

Sarkar, S., Blaney, L.M., Gupta, A., Ghosh, D., SenGupta, A.K., 2008. Arsenic Removal from Groundwater and Its Safe Containment in a Rural Environment: Validation of a Sustainable Approach. Environ. Sci. Technol. 42 (12), 4268–4273.

Schaefer, M.V., Ying, S.C., Benner, S.G., Duan, Y., Wang, Y., Fendorf, S., 2016. Aquifer Arsenic Cycling Induced by Seasonal Hydrologic Changes within the Yangtze River Basin. Environ. Sci. Technol. 50 (7), 3521–3529.

Schideman, L.C., Mariñas, B.J., Snoeyink, V.L., Campos, C., 2006. Three-Component Competitive Adsorption Model for Fixed-Bed and Moving-Bed Granular Activated Carbon Adsorbers. Part II. Model Parameterization and Verification. Environ. Sci. Technol. 40 (21), 6812–6817.

Scott, T.B., Allen, G.C., Heard, P.J., Randell, M.G., 2005. Reduction of U(VI) to U(IV) on the surface of magnetite. Geochim. Cosmochim. Acta 69 (24), 5639–5646.

SenGupta, A.K., 2017. Ion Exchange in Environmental Processes: Fundamentals, Applications and Sustainable Technology. John Wiley & Sons, pp. 224–296.

SenGupta, A.K., German, M., Chatterjee, P., Shaw, A., Sarkar, S., Watkins, T.A., Rahman, M., Chowdhury, M., 2017. Breakthrough Technology or Breakthrough Solution: What Are We Really After? Environ. Sci. Technol. 51 (5), 2529–2530.

Sherman, D.M., Randall, S.R., 2003. Surface complexation of arsenic(V) to iron(III) (hydr)oxides: structural mechanism from ab initio molecular geometries and EXAFS spectroscopy. Geochim. Cosmochim. Acta 67 (22), 4223–4230.
Tresintsi, S., Simeonidis, K., Estradé, S., Martinez-Boubeta, C., Vourlias, G., Pinakidou, F., Katsikini, M., Paloura, E.C., Stavropoulos, G., Mitrakas, M., 2013. Tetravalent Manganese Feroxyhyte: A Novel Nanoadsorbent Equally Selective for As(III) and As(V) Removal from Drinking Water. Environmental Science & Technology 47 (17), 9699–9705.
Wang, Z., Hu, W., Kang, Z., He, X., Cai, Z., Deng, B., 2019b. Arsenate adsorption on iron-impregnated ordered mesoporous carbon: Fast kinetics and mass transfer evaluation. Chem. Eng. J. 357, 463–472.
Wang, C., Luan, J., Wu, C., 2019a. Metal-organic frameworks for aquatic arsenic removal. Water Res 158, 370–382.
Westerhoff, P., Highfield, D., Badruzzaman, M., Yoon, Y., 2005. Rapid Small-Scale Column Tests for Arsenate Removal in Iron Oxide Packed Bed Columns. J. Environ. Eng. 131 (2), 262–271.
Wolthers, M., Charlet, L., van Der Weijden, C.H., van der Linde, P.R., Rickard, D., 2005. Arsenic mobility in the ambient sulfidic environment: Sorption of arsenic(V) and arsenic(III) onto disordered mackinawite. Geochim. Cosmochim. Acta 69 (14), 3483–3492.
Wu, Z., Webley, P.A., Zhao, D., 2010. Comprehensive study of pore evolution, mesostructural stability, and simultaneous surface functionalization of ordered mesoporous carbon (FDU-15) by wet oxidation as a promising adsorbent. Langmuir 26 (12), 10277–10286.
Xie, S., Yuan, S., Liao, P., Tong, M., Gan, Y., Wang, Y., 2017. Iron-Anode Enhanced Sand Filter for Arsenic Removal from Tube Well Water. Environ. Sci. Technol. 51 (2), 889–896.
Yan, Z., Flanagan, S.V., 2017. The Case for Universal Screening of Private Well Water Quality in the U.S. and Testing Requirements to Achieve It: Evidence from Arsenic. Environ. Health Perspect. 125, 1–6.
Yang, W., Kan, A.T., Chen, W., Tomson, M.B., 2010. pH-dependent effect of zinc on arsenic adsorption to magnetite nanoparticles. Water Res 44 (19), 5693–5701.
Yang, W., Zhao, N., Zhang, N., Chen, W., Kan, A.T., Tomson, M.B., 2012. Time-dependent adsorption and resistant desorption of arsenic on magnetite nanoparticles: kinetics and modeling. Desalin Water Treat 44 (1-3), 100–109.
Yu, Q., Zhang, R., Deng, S., Huang, J., Yu, G., 2009. Sorption of perfluorooctane sulfonate and perfluorooctanoate on activated carbons and resin: Kinetic and isotherm study. Water Res 43 (4), 1150–1158.
Zhang, X., Wu, M., Dong, H., Li, H., Pan, B., 2017. Simultaneous Oxidation and Sequestration of As(III) from Water by Using Redox Polymer-Based Fe(III) Oxide Nanocomposite. Environ. Sci. Technol. 51 (11), 6326–6334.
Zhao, X., Liu, W., Cai, Z., Han, B., Qian, T., Zhao, D., 2016. An overview of preparation and applications of stabilized zero-valent iron nanoparticles for soil and groundwater remediation. Water Res 100, 245–266.